# Impacts of a capillary barrier on infiltration and subsurface stormflow in layered slope deposits monitored with 3D ERT and hydrometric measurements

Rico Hübner[1], Thomas Günther[2], Katja Heller[1], Ursula Noell[3], and Arno Kleber[1]

[1]Institute of Geography, Dresden University of Technology, Helmholtzstr.10, 01069 Dresden, Germany
[2]Leibniz Institute for Applied Geophysics (LIAG), Stilleweg 2, 30655 Hannover, Germany
[3]Federal Institute for Geosciences and Natural Resources (BGR), Stilleweg 2, 30655 Hannover, Germany

*Correspondence to:* R. Hübner (rico.huebner@tu-dresden.de)

**Abstract.** Identifying principles of water movement in the shallow subsurface is crucial for adequate process-based hydrological models. Hillslopes are the essential interface for water movement in catchments. The shallow subsurface on slopes typically ~~consist~~ of different layers with varying characteristics. The aim of this study was to draw ~~conclusion~~ about the infiltration behaviour, to identify water flow pathways and derive general validity about the water movement on a hillslope with periglacial slope deposits (cover beds), where the layers differ in their sedimentological and hydrological properties. Especially the described varying influence of the basal layer (LB) as impeding layer on the one hand and as a remarkable pathway for rapid subsurface stormflow on the other. We used a time lapse 3D ERT approach combined with punctual hydrometric data to trace the spreading and the progression of an irrigation plume in layered slope deposits during two irrigation experiments. This multi-technical approach enables us to connect the high spatial resolution of the 3D ERT with the high temporal resolution of the hydrometric devices. Infiltration through the uppermost layer was dominated by preferential flow, whereas the water flow in the deeper layers was mainly matrix flow. Subsurface stormflow due to impeding characteristic of the underlying layer occurs in form of "organic layer interflow" and at the interface to the first basal layer (LB1). However, the main driving factor for subsurface stormflow is the formation of a capillary barrier at the interface to the second basal layer (LB2). The capillary barrier prevents water from entering the deeper layer under unsaturated conditions and diverts the seepage water according to the slope inclination. With higher saturation the capillary barrier breaks down and water reaches the highly conductive deeper layer. This highlights the importance of the capillary barrier effect for the prevention or activation of different flow pathways under variable hydrological conditions.

## 1 Introduction

Analyses of flood frequencies over the last decades in Europe and other parts of the world reveal a positive trend which is predicted to be continued (Zhang et al., 2016; Alfieri et al., 2015; Schmocker-Fackel and Naef, 2010; Uhlemann et al., 2010; Petrow and Merz, 2009). Flood forecasting and predicting water quantity and quality under alternating boundary conditions is usually performed by hydrological modelling. The knowledge of internal catchment response and different feedback mecha-

nisms is decisive for an increased process understanding and an accurate modelling of the hydrological behaviour (Seibert and van Meerveld, 2016). Therefore, it is essential to comprehend the reactions in the watersheds.

Water dynamics in catchments and the response to temporally and spatially variable climatic and hydrological conditions are of particular importance to runoff generation. For watershed processes hillslopes are the crucial interface between precipitation and runoff. With their structure and properties they decisively determine the separation in different runoff components, and they control water movement and flow pathways within catchments. Several studies have addressed hillslope hydrology (Uchida et al., 2006; McDonnell et al., 2001; Anderson and Burt, 1990; Kirkby, 1980).

Most of the studies focused on hillslopes hydrology concluded that the internal water flow is linked to the structure of the subsurface as well as the pre–event conditions for different runoff situations (Uhlenbrook et al., 2008; Wenninger et al., 2004). The shallow subsurface is one of the most heterogeneous and complex parts in natural landscapes causing a highly variable spatial and temporal hydrological response. Understanding the ongoing processes, generalizing and transferring observations by developing new theories and approaches for prediction are key features to improve hydrological models (McDonnell, 2003).

Various slopes are featured with layered structure, due to different soil or sedimentological layering. The major near-surface solid material on mid-latitude hillslopes are slope deposits (Kleber and Terhorst, 2013; Semmel and Terhorst, 2010). The properties of these Pleistocene periglacial cover beds are significantly influenced by the parent material and may generally be divided into three main layers depending on age and genesis (Kleber and Terhorst, 2013; Völkel et al., 2002). The uppermost layer, the "upper Layer" (LH), is a quasi-ubiquitous 0.4 to 0.6 m thick layer with low bulk density and high biotic activity. The underlying "intermediate layer" (LM), with higher bulk density and a significant aeolian component, varies in thickness and typically contains less coarse clasts than the other layers. The deepest layer, the "basal layer" (LB) consists of relocated local bedrock material, usually with a high amount of clasts and no appreciable aeolian influence. LM and LB may have developed a multi-part structure.

Many prior studies confirm the influence of cover beds for near-surface water balance (infiltration, storage and percolation) and runoff, e.g., subsurface stormflow (Heller and Kleber, 2016; Hübner et al., 2015; Moldenhauer et al., 2013; Chifflard et al., 2008; Völkel et al., 2002; Sauer et al., 2001; Kleber and Schellenberger, 1998). The hydrological response to precipitation mainly depends on their sedimentological and substrate-specific properties, such as grain-size distribution, clast content and texture as well as the pre–event condition.

Flow pathways within the layers vary due to the local situation and may develop in different layers or rather along layer interfaces. In general, precipitation may easily enter the porous, macropore-rich and highly conductive LH and percolate to the interface with the LM. As a consequence of the lower hydraulic conductivity and higher compaction of the LM the interface should form a temporary barrier and cause interflow. A few studies may evidence lateral flow on this interface, due to impermeable zones of the LM, whereas other studies record backwater within the LM, causing interflow at the interface to the LB (Heller and Kleber, 2016; Chifflard et al., 2008). Whether the LB acts as an impeding layer depends on the parent material. With clay-rich bedrock, sandstone or red bed the LB may be developed as an aquiclude and on the contrary with granitic, slate, shale or gneiss bedrock the LB may act as an aquifer (see Moldenhauer et al. (2013), and references therein).

Several authors (Heller and Kleber, 2016; Chifflard et al., 2008; Sauer et al., 2001; Kleber and Schellenberger, 1998) describe the LB as a layer with reduced vertical percolation of seepage water. Additionally, the hydraulic properties of the LB are to be referred to as anisotropic, with low vertical but high lateral hydraulic conductivity. Whether the seepage water is able to enter the LB or not is attributed to the initial conditions. With high pre-moisture, precipitation or snow melt water may enter the LB and cause a rapid increase of subsurface stormflow. The reaction of LB as an aquitard in vertical direction on the one side and as temporary aquifer for lateral runoff under moist conditions on the other side and how the water enters the LB is not fully understood.

Most of the studies were based on invasive and extensive hydrometric point measurements or on tracer investigations. Hydrometric measurements may modify flow pathways and because of their commonly punctual record they are not sufficient in the case of considerably spatial heterogeneity in the subsurface. Tracer experiments provide less direct insights into ongoing processes. The internal hydrological behaviour may be complex and nonlinear and due to the spatio-temporal interlinking of different processes, there are still numerous knowledge gaps and missing generalization and transferability regarding runoff generation in watersheds (Ali et al., 2015; Tetzlaff et al., 2014; McDonnell, 2003).

Today, state-of-the-art measurement methods e.g. hydrogeophysical methods such as ERT (*Electrical Resistivity Tomography*) are capable to measure resistivity changes correlated with subsurface water flow with high resolution on different spatial or temporal scales. ERT is a commonly used application in subsurface hydrology studies, e.g., infiltration (e.g., Hübner et al., 2015; Ganz et al., 2014; Travelletti et al., 2012; Cassiani et al., 2009; Singha and Gorelick, 2005; French and Binley, 2004; Descloitres et al., 2003; Michot et al., 2003), imaging water flow with tracer on a field scale (e.g., Scaini et al., 2017; Doetsch et al., 2012; Kuras et al., 2009; Kemna et al., 2002; Ramirez et al., 1993) or laboratory scale (e.g., Bechtold et al., 2012; Garré et al., 2010; Koestel et al., 2008; Binley et al., 1996). They close the gap between large-scale depth-limited remote-sensing methods and invasive punctual hydrometric arrays at the field scale (Robinson et al., 2008a, b; Uhlenbrook et al., 2008; Lesmes and Friedman, 2006). This is essential to better cope with the problem of heterogeneity and complexity within hillslope hydrology.

Besides explicit characterization of landscape heterogeneities it is crucial to identify the principles that underlie the heterogeneity and complexity (McDonnell et al., 2007). The intention should not be to produce high resolution data with only local validity, but rather use this data to gain a better understanding of the ongoing processes that may be transferred fundamentally to ungauged basins.

The aim of this study is to monitor water movement in the vadose zone on a hillslope with a typical three-layer profile during an irrigation experiment. Due to the different sedimentological and, accordingly, hydrological properties and also the spatial heterogeneity of the individual layers, the water movement may be very complex. A minimally invasive 3D ERT surface array with continuous time lapse measurements help to analyse flow pathways within the layers. Additional tensiometers were used to validate the ERT models and to show exact breakthrough curves.

The major objectives are to show different behaviour of the layers relating to infiltrating water under various initial conditions (low and high antecedent moisture) . Based on the properties described in previous studies (see above), the LH is expected to be highly conductive and characterized by preferential flow. The high resolution 3D ERT should help to confirm this assumption. The behaviour of the LM and LB are discussed contradictorily. The less conductive LM is often described as one of the main

~~layer~~ for subsurface stormflow. In contrast, the coarse and, therefore highly conductive LB has been depicted as hydrologically very variable according to time and conditions. One of the major ~~objective~~ is to show, whether the seepage water is impeded by the LM or LB and which are the main layers for lateral flow. Furthermore, we address the question which conditions or limitations trigger or hinder the seeping of water into the coarse grained LB? This includes to analyse principles of water movement in cover beds and give explanations of the subsurface runoff due to the different sedimentological or hydrological properties as grain size distribution, bulk density and hydraulic conductivity.

## 2 Material and Methods

### 2.1 Study site and subsurface properties

The study site is located on a hillslope of a well-studied headwater catchment (6 ha) in the Eastern Ore Mountains. For general information as well as electrical characteristics of the investigation area we refer to Heller and Kleber (2016); Hübner et al. (2015); Moldenhauer et al. (2013). The plot monitored in this study is situated on a slope at an altitude of 535 m asl. with a north-east aspect in direction to one of the contour lines of the catchment. This 15 ° inclined plane slope is covered with a typical three-layer profile (LH, LM and LB) and underlying biotite gneiss. It is forested mainly with spruce (*Picea abies (L.) Karst*) and sporadic European beech (*Fagus sylvatica*). Undergrowth is not evident in this particular area. The ~~organic matter~~ mainly consists of moderate decomposed spruce needles overlain by a continuous thin layer of dry beech leaves from last fall. The soil type is a Stagno-Gleyic Camibisol. Several sedimentological data have already been determined in previous studies (see Heller and Kleber, 2016; Hübner et al., 2015). Because those data only represent average values for the catchment, their validity for the experimental plot in particular is restricted. Therefore, hydraulic conductivity, bulk density and grain size distribution were additionally determined at the exact location of the experiment. Hydraulic conductivity was measured with a compact constant-head permeameter (Anemometer–Eijkelkamp) and calculated using the Glover analytic solution (Zangar, 1953). Additional soil cores extracted from different depths were analysed with a multistep outflow method in the laboratory. In this type of surveys, grain size is often divided at 2 mm, with the soil texture on the one side and clasts on the other. Because not only the distribution of the fine soil is important for the water movement, we want to analyse the distribution of the entire range across all grain sizes without the division at 2 mm. Therefore, the particle-size distribution $\geq 0.063$ mm was determined by sieving and for $\leq 0.063$ mm by sedimentation method (DIN 18123 (1983) with the sand–silt limit at 0.063 mm). Percentage of different grain size scales was calculated as weight percentage per total sample weight.

### 2.2 Irrigation experiment

The experiment was performed on a plot approx. 3x8 m equipped with tensiometers and ERT surface electrodes (Fig. 1). Downslope a trench was excavated down to 1.5 m to detect potential lateral flow from upslope. This allowed a better sampling and characterizing of the subsurface. A tent was placed over the lower part to protect this area from direct rainfall. Therefore, a reaction beneath the rain-protected area is only possible by lateral flow. During the investigation period from May 27, 2015 to

June 1, 2015 we performed two irrigation experiments on May, 27 (290 min) and May, 29 (275 min) with a rainfall intensity of 62 and 68 mm/h, respectively. Within the irrigated plot of 1.5 x 1.5 m the beech leaves were removed, because during earlier tests they induced short overland flow and we wanted to monitor the water movement within the subsurface starting on top of the soil (not on the leaf litter). To ensure a uniform precipitation intensity we used a mobile sprinkling device with 60 pressure equalized drip heads arranged in a row constantly moving over the irrigation plot on two parallel rails 0.6 m above the surface. The water used for the irrigation was extracted from the nearby spring and thus ensured comparable properties (temperature and electrical conductivity) as the pore water of the subsurface so that dissolution processes can be neglected. Furthermore, dissolution processes hamper only the quantitative assessment of the subsurface flow using ERT but this is not attempted in this study. For continuous recording of hydrometric data, 20 tensiometers ((UMS – T8) in four groups of five per group were installed at 1.5 and 2.5 m downslope of the irrigation area (see Fig. 1). Within each distance two tensiometer groups were arranged at depths of 0.3, 0.6, 0.85, 1.2 and 1.5 m. They recorded matric potential ($\Psi_m$) and temperature simultaneously with a temporal resolution of 1 min. Additionally, one tensiometer was installed in the trench reaching a depth of 2.5 m.

## 2.3   3D time lapse ERT

Electrical resistivity tomography (ERT) has become an established method for minimally invasive three-dimensional characterization of moisture content in laboratory soil samples (e.g. Garré et al., 2010) or in the subsurface (e.g. Beff et al., 2015), once a relationship of resistivity ~~and~~ substrate parameters is established. It is of particular importance for monitoring hydrological processes in the subsurface with high temporal resolution. Modern instruments allow connecting several hundreds of electrodes, placed either at the surface or installed in the ground. Multi-channel instruments allow thousands of four-point measurements per hour, of which two electrodes are used for current injection and two others for electric potential measurement. An inverse problem is solved to reconstruct the subsurface resistivity distribution (Günther et al., 2006). Beff et al. (2015) describe the whole data flow in a hydrological context, including the pedoelectrical transformation and the validation by TDR measurements. The horizontal spatial resolution of small-scale measurements depends mainly on the electrode distance, but decreases vertically. The vertical resolution can be significantly improved by installing subsurface ring electrodes (Beff et al., 2015). However this was not possible without destroying the slope deposits, which is why we ~~decided on~~ a pure surface measurement with a very dense electrode layout dedicated for multi-channel measurements that kept the temporal resolution high.

To image the plume beneath and downslope of the irrigated area, a 3D surface ERT array (2.8x5.6 m) was installed perpendicular to the slope inclination. The upper part includes 196 electrodes with a spacing of 0.2 m for a correspondingly high resolution in proximity to the irrigated plot. In the lower part a 0.2 m grid was used in a checker-board style, i.e., every second point was not used thus leading to dipoles of 0.4 m, but skewed electrode distances of 0.28 m. This involved 98 electrodes covering a wider area with a fast acquisition time, however with reduced spatial resolution. This trade-off was chosen due to the maximum possible electrode number of 300.

Analysis of ERT data, particularly when using small electrode distances, requires accurate determination of electrode positions to avoid positioning errors. Therefore, the shape of the surface and the exact position of all sensors were surveyed with a total station (Leica TPS1200).

We used the instrument GeoTom by Geolog instruments (http://www.geolog2000.de) with six measuring channels, i.e. simultaneous voltage measurements per current injection, if adequate electrode arrays (dipole-dipole or multi-gradient) are used. The maximum current is $100\,\mathrm{mA}$ but for these measurements the current was fixed to $1\,\mathrm{mA}$. For the survey we used a low frequency of $4.167\,\mathrm{Hz}$. There is a large number of different measuring protocols even for 2D ERT, and much more for 3D ERT. We organized the electrodes in three electrode grids (s. Fig. 1a): the 14x14 grid (blue) in the upper part with $0.2\,\mathrm{m}$ spacing and two staggered grids (red and green) of each 7x13 electrodes in $0.4\,\mathrm{m}$ spacing covering the whole area. We decided for the dipole-dipole array as it provides the highest spatial resolution (Friedel, 2003) and it is efficiently applied in multi-channel operation. In each grid, every pair of neighbouring electrodes was used for current injection. Additionally, we injected currents through the two outermost electrodes of each line for increasing penetration depth, resulting in a so-called circular dipole-dipole array (Friedel, 2003). Potentials were measured between adjacent electrodes along the same line (radial dipole array) and along the neighbouring lines (equatorial dipoles) in both $x$ and $y$ directions.

As temporal resolution is crucial, redundancy in terms of reciprocal data was widely avoided and only included for filling up the measuring channels. This resulted in a total number of 475 current injections with 6 potential measurements each, so that a total number of 2850 data was measured. Between three and eight repetitions were made for each current injection until the standard deviation of the potential differences was below 2%. This resulted in a mean measuring time of about $4\,\mathrm{s}$ for each current injection and thus a total time of about $25\text{-}30\,\mathrm{min}$ for each time frame. The time frame repetition rate was fixed to $35\,\mathrm{min}$ before the measurement, and the instrument measured automatically for a period of fours days and 18 hours. In total, 197 frames have been measured, resulting in about 560,000 data points for the whole period.

The time frames were considered to represent single states that are temporally associated 14 min after the beginning of the individual measurements. One electrode was not working properly so that all corresponding measurements had to be deleted.

For inversion, we used the BERT (Boundless Electrical Resistivity Tomography) code. The numerical details of the underlying forward and inversion problems are described by Rücker et al. (2006) and Günther et al. (2006), respectively, for the steady-state problem. The time-lapse inversion represents a subsequent inversion of the individual timestep data, but with the initial model used as a reference model. In order to account for systematic errors (e.g., from positioning inaccuracies), the initial misfit vector was removed from the subsequent data. Bechtold et al. (2012) describe this procedure referred to as difference inversion (see LaBrecque and Yang (2001)) for ERT monitoring of moisture transport in a synthetic laboratory soil. For weighting the individual data we used an error estimate consisting of a percentage of 3% and a voltage error of $10\,\mu\mathrm{V}$, these values are known from experience for this instrument and acquisition. As a result, readings with low voltage gain obtained less weight. However, the effect of the voltage error is relatively small. As a remarkable part of the data is systematic and thus removed in the difference inversion, we decreased the percentage error to 1% for the timelapse inversion, which was reached for most frames except some with erroneous data.

The parameter mesh was chosen fine enough to account for small-scale changes, so that the resistivity distribution is represented by 75,000 tetrahedra. We used lower and upper resistivity bounds of 100 and $4000\,\Omega\mathrm{m}$ to keep the resistivity in a reasonable range. First-order smoothness with slightly anisotropic penalty for the vertical direction (a factor of 0.2) was used

for regularization. The regularization factor $\lambda$ determining the influence of the roughness was chosen higher for the baseline model (100) and decreased for the time steps (30) to fit the data within error estimates.

Comparing resistivity betweens different depths and different time steps, the subsoil temperature profile (e.g., depth depending temperature, daily and long time variations) had to be taken into account. For the investigation period ~~is~~ the time depending temperature variation (max. $0.78\,°C$) smaller compared to the change with depth (max. $1.64\,°C$). The temperature-depth profiles from the hydrometric data have been used for each ERT time step enabled to correct resistivity ($\rho_t$) at in-situ temperature ($T$) to resistivity at a soil temperature of $25\,°C$ ($\rho_{25}$) for all depth using Eq. (1) as proposed in Keller and Frischknecht (1966):

$$\rho_{25} = \rho_t \left(1 + \delta \left(T - 25\right)\right) \tag{1}$$

The empirical parameter $\delta$ is the temperature slope compensation, with $\delta = 0.025\,°C^{-1}$ being commonly used for geophysical applications (Keller and Frischknecht, 1966; Hayashi, 2004; Ma et al., 2011). Instead of correcting measured apparent resistivities we invert for in-situ (temperature-dependent) resistivity and correct the inversion results to mean temperature before further analysis.

## 3   Results

### 3.1   Subsurface structure and physical properties

The LH has a very low bulk density, contains organic components (roots etc.) and shows high biotic activity. Soil texture is classified as silt loam with a moderate amount of clasts (Table 1). The LH ~~provides~~ a relatively constant thickness of $0.5\,m$ over the entire area. Due to the considerable amount of macropores and its low bulk density, the LH is a ~~well~~ permeable layer (Table 1). Due to the high hydraulic conductivity, which is even higher in the organic matter, water may easily enter the LH, overland flow is not evident in the study area.

The LM ($\approx 0.5$–$0.8\,m$) consists of a substratum similar to the LH (soil texture $\equiv$ silt loam) but with a higher bulk density and an increased amount of aeolian components (see Fig. 2: coarse silt and fine sand). Apart from some root channels the macropores are reduced which decreases the hydraulic conductivity to $65\,cm\,d^{-1}$ (Table 1). At the interface between the LM and the LB1 at $\approx 0.8\,m$ depth the composition of the finer grain sizes changes from a dominance of silt to coarser fractions such as medium and coarse sand (Fig. 2). Accordingly, the soil texture of the LB1 is a sandy loam with an even higher bulk density, less porosity and slightly higher amount of clasts (Table 1). It reaches an average depth of $1.1\,m$. This depth range is characterized by the lowest hydraulic conductivity and by hydromorphic (stagnic) properties which indicate substantial temporal changes in water saturation.

The underlying LB2 is composed of up to decimetre–scale angular platy debris and a very low amount of fine soil. The clasts are often laterally bedded with longitudinal axes oriented parallel to the slope. At the flat bottom of the clasts fine material may be entirely absent. Blank undersides of rock fragments indicate strong water flow in the pores between the clasts (Moldenhauer et al., 2013). The bulk density and hydraulic conductivity of this material could not be accurately determined by measurements.

Due to the huge amount of coarse clasts it was not possible to extract representative soil cores. Permeameter measurements were not feasible because the hydraulic conductivity of the LB2 exceeds the maximum outflow rate of $3 \times 10^{-6}\,\mathrm{m^3\,s^{-1}}$. A rough estimate from an infiltration measurement in a borehole at the bottom of the trench yielded a hydraulic conductivity of $> 2 \times 10^3\,\mathrm{cm\,d^{-1}}$ (Table 1).

## 3.2 Irrigation experiments

### 3.2.1 Initial conditions and baseline model

The average throughfall of the study area in May 2015 was approx. $24\,\mathrm{mm}$. In the last two weeks before the experiment, less than $4\,\mathrm{mm}$ of rain was recorded. In combination with the increasing evapotranspiration in the spring season, the initial conditions of the subsurface were rather dry. This corresponds with the average resistivity profile of the irrigation plot as well as the average matric potentials (Fig. 3). The LH is characterized by two different depth ranges. At shallow depths ($< 0.3\,\mathrm{m}$), the resistivity is considerably lower than in the deeper parts ($0.3$ to $0.5\,\mathrm{m}$). Near the interface to the LM (approx. $0.5\,\mathrm{m}$) the highest resistivity correlates with the lowest matric potential of the subsurface. With increasing depth, resistivity decreases continuously from $1100\,\Omega\mathrm{m}$ to $550\,\Omega\mathrm{m}$. The lowest values were detected in the LB2 where the decreasing trend slightly proceeded with depth but not as pronounced as in the LM and the LB1. The layers also show a significant difference in the variance of the resistivity values. The boxplot clearly illustrates a decreasing variability with depth (Fig. 3). The LB2 has a very low variability, in contrary to the considerably high variability of the LH.

The depth profile of the matric potentials shows a comparable but reverse trend. The highly negative values at $0.3\,\mathrm{m}$ depth continuously increase with depth. In the LB2 only slight changes are noticeable down to $2.5\,\mathrm{m}$ (-50 to 47 hPa). Due to the punctual characteristics of the hydrometric measurement, there are some details missing in the depth profile that are evident in the ERT results. For example the uppermost part of the resistivity profile is characterized by low values, which may be due to antecedent rainfalls and different material properties (e.g. organic matter and higher humus content). The installation depth of the shallowest tensiometers does not match this part of the very low resistivity values and, therefore, was possibly not traced by the matric potential values. Considering only the punctual information of the tensiometers, the depth profile would be interpreted as continuous increase. However, the ERT data indicate a trend reversal at $0.5\,\mathrm{m}$ depth. Above and below this depth the trends are quite the opposite. However, the reason for this low resistivity near the surface needs to be investigated in detail in order to exclude inversion artefacts. 

### 3.2.2 Hydrological correlation

Comparing the data from ERT and matric potential measurements by means of time series at points at different depths downslope, both methods show good agreement of results (Fig 4 and Fig 5). The resistivity changes observed by ERT imply an earlier and smoother breakthrough than the changes of matric potential. Due to the lower temporal resolution and due to the smoothing in the inversion, it is not possible to derive the exact breakthrough curves. These may be derived from the hydrometric data. Since the tensiometers are installed at different depths downslope of the irrigation area, a change in matric potential is only

possible by lateral water transport from upslope direction. The depth ranges of the two different distances (1.5 and 2.5 m) to the irrigation plot differ in the magnitude of reaction and in the response time. Except for the progression of the curve at 0.3 m, all other depths provide sharp responses and the reactions due to lateral water movement are precisely determinable.

Since the deepest tensiometers are installed in a very coarse material the interpretation of matric potential may be difficult. We assume that due to the portion of small grain sizes and the huge amount of irrigation water at least a minimal contact to the surrounding pores may register a start of change in moisture content. Even without any contact to the surrounding matrix, the tensiometers should operate as piezometers. In accordance to the resistivity values, we are convinced that it is possible to interpret significant points of the matric potential time series. Tab 2 and Tab 3 illustrate for both irrigation experiments the start  of the breakthrough (time from start of the irrigation to the start of changes in moisture), the time to saturation (time from start of the irrigation until the achievement of saturation $\approx 0\,\mathrm{hPa}$) and the end of the breakthrough (time from start of the irrigation until the apex of the matric potential curve).

The amount of precipitation of both the first and the second irrigation experiment induced lateral water flow which caused a clear reaction of all tensiometers at 1.5 m distance downslope. The spread of water at shallow depth has no significant lateral component. Only a slight spreading of water mainly downslope within the organic matter could be observed visually during the irrigation. This is also indicated by the matric potential data. It lasts almost until the end of the irrigation (approx. 4 h cf. Table 2) to cause a reaction at 0.3 depth 1.5 m downslope. Compared with other depths the change is rather gradual and smooth (Fig 4). During the second irrigation the increase continued gradually with no major changes (Fig 5). Despite the increase in water content, the saturation after the experiment was still quite low as evidenced by a low matric potential.

The matric potential at 0.6 m depth did already respond 1 h 40 min after the start of the first irrigation (Tab. 4). Similarly to the ERT data the tensiometers, show a clear and fast reaction, and at the end of the first irrigation the saturation has already been achieved. The response to the second irrigation experiment is comparable, but due to the moister pre–conditions the entry times are significantly faster (Tab. 3). While in the first experiment the steady state conditions were achieved only for a few minutes, the total saturation lasted 2 h 30 min during the second one.

The time series at 0.85 m depth shows a similar trend as at 0.6 m but with a delay of approx. 30 min (Tab. 3). Due to the moist initial conditions, the rapid saturation and the sufficient large amount of water, even a minor pressure potential is recorded during the second irrigation indicating backwater (Fig. 5).

At 1.2 and 1.5 m depth comparable breakthrough times are registered, which start off simultaneously with the time of saturation at shallow depths (Tab. 2). In comparison to the overlying layers, the changes are smaller. Taking into account the initially low matric potential and different resistivity–saturation relationship at this depth (see Archie parameters in Hübner et al. (2015)) comparatively high matric potentials have been achieved (Fig. 4). But in contrast to 1.2 m, which shows a pressure potential by the second irrigation similar to the 0.85 m depth, no saturation could be reached in 1.5 m during both irrigations.

During the first experiment there was a considerable reaction at the 1.5 m distance, but almost none at 2.5 m down the slope (Fig. 5). In contrast, the second irrigation triggered an evident response within the second distance. This furthest downslope orientated spread of the irrigation water is limited to the LM and the LB1 at 0.6 and 0.85 m depth, respectively. At 0.6 m depth

it lasts 2 h from the breakthrough within the first distance to the breakthrough within the second distance, while it lasts almost 4 h at 0.85 m depth (Tab. 3).

### 3.2.3 3D time lapse ERT

The change of resistivity is observed nearly instantly at the irrigation plot and propagates into the subsurface with time. The volumes of the subsurface which are affected by different amounts of changes of resistivity may be represented by plumes of different resistivity ratios. To visualize the 3D extent of the plumes, the contour surfaces (equal resistivity ratios in reference to the baseline model) at different time steps in a profile view and the corresponding top view are shown in Fig. 6 for the first irrigation and Fig. 7 for the second irrigation.

The change of resistivity in the LH does not start from the surface as a single plume but as concentrated changes along separated parts (Fig. 6 - 25 min). After 1 h large parts of the LH show a strong decrease of resistivity down to the interface to the LM. The resistivity changes proceed heterogeneously. There still are different zones of minor resistivity changes. By contrast, the resistivity changes within the LM and the LB1 extend relatively homogeneously until the plume reaches the interface to the LB2 in approx. 1.1 m (Fig. 6 - 60 min). The interface acts as barrier and forms the vertical boundary for infiltrating water. Subsequent to the vertical spread, the plume is deflected in a lateral direction following the slope inclination (Fig. 6 - 130 min). This lateral downslope spreading is mainly limited to the LM and the LB1 in 0.5 to 1.1 m depth. No significant lateral component is shown at shallow or greater depth. During the experiments no changes were recorded in the LB2 below the irrigation area. Only further downslope the changes extend vertically into the LB2 (Fig. 6 - 305 min).

Immediately after the completion of the first irrigation no further spread of the plume is indicated. The spatial extent continuously shrinks until the beginning of the second irrigation (Fig. 7 - initial). The initial conditions of the second irrigation are characterized by significantly lower resistivity of the LH (esp. < 0.3 m) below the irrigation area and lower resistivity of the LM and the LB1 below the irrigation area and downslope. The propagation direction of the zone with decreased resistivity during the second irrigation is identical to the propagation direction during the first irrigation. Initially a vertical movement dominates until the plume reaches the interface to the LB2 (Fig. 7 - 47 min). Subsequently, the plume is laterally deflected downslope (Fig. 7 - 82 min). The water flow indicated by the resistivity decrease during the second irrigation is considerably faster than during the first experiment. Already after 2 h the final conditions of the first irrigation are re-established. As a result the plume may extend further downslope (Fig. 7 - 292 min).

In general, the test area may be differentiated into two separate areas with different changes in resistivity. The area right beneath the irrigation plot, which is characterized by fast vertical changes down to a maximum depth at the interface to the LB2 (Fig. 8). On the other hand, the area downslope of the irrigation plot is characterized by laterally induced changes in the LM and the LB1 and subsequent vertical extend into the LB2 (Fig. 9).

## 4 Discussion

As pointed out previously, using only the ERT time lapse models it is difficult to determine accurate breakthrough times, but the trend and the amount of the change due to subsurface water movement may be reproduced very well by changes in resistivity. The advantage of the 3D ERT is the significantly higher spatial resolution compared to the tensiometers. Combining hydrometric data and the results from the ERT time lapse measurements it is possible to get an insight into the infiltration process and the 3D subsurface water movement. Because of the resistivity temperature correction, changes in resistivity may only be caused by changes in conductivity or amount of pore water. Decreasing resistivity may be interpreted as increased saturation.

Owing to the loose bedding and the high hydraulic conductivity of the LH, overland flow could not be evidenced on the test plot. A slow downslope expansion of water mainly due to gravity, wettability and adhesion/adsorption (attraction of solid surfaces) within the organic matter could be observed visually during the irrigation. The infiltration at the surface is not limited to the irrigated area. The infiltration area seems to extend into downslope direction. This may be caused by organic layer interflow at the mineral soil interface which percolates into the LH after a short distance downslope. This kind of interflow could also be observed by Heller and Kleber (2016) in the study area.

Due to the high porosity and the dry initial conditions the LH beneath the irrigation plot is characterized by the highest increase in moisture as indicated by the highest changes of resistivity. The infiltration into the LM proceeds very rapidly but spatially not uniform. Due to the heterogeneous structure, the flow regime of the LH is dominated by preferential flow pathways. These preferential areas are still moderately evident at the beginning of the second irrigation experiment. Along these preferential pathways, the seepage water quickly reaches the interface to the LM. An impeding effect of the less hydraulically conductive and dense LM could not be detected. Therefore, a subsurface stormflow at the interface to the LM may be excluded. In contrast to the LH, there is no evidence for preferential flow within the LM. The spread of resistivity change into the subsurface is rather uniform, suggesting a propagating wetting front. However, the reduced spatial resolution at the depth of the LM and the smoothness constrain of the inversion procedure may have obscured smaller preferential pathways at the depth of the LM.

During the early infiltration the orientation of the flow vector is in the upslope direction[1] (Fig. 6 - 60 min). Sinai and Dirksen (2006) described with laboratory experiments for an unsaturated homogeneous slope that the flow direction during early wetting may be directed upslope and during a flow regime of steady infiltration, the flow vector is changed toward the vertical direction. Already after 1 h 35 min a clear change of the orientation into the vertical direction is recognizable (Fig. 6 - 95 min).

Due to the higher density, lower hydraulic conductivity and porosity, only a part of the seepage water may percolate into the LB1. A small portion of the water is diverted downslope initially (Fig. 6 - 130 min). This induces a first subsurface stormflow at the interface between the LM and the LB1 and correlates well with the results from the matric potential measurements at 1.5 m distance (Fig. 4). The depth range of the LM (0.6 m ≈ 1 h 40 min) shows the first reaction due to lateral water movement.

---

[1]here we define downslope and upslope relative to the vertical as described by Philip (1991)

Despite the inhibiting effect of the LB1, most of the water percolates into this layer down to the interface of the LB2. The interface of the LB2 acts as a barrier for the seepage water. During the whole experiment no change were measured within depths >1.1 m right beneath the irrigation area (Fig. 8). Although the LB2 is a highly conductive coarse material, the water does not enter this layer there.

Gardner and Hsieh (1959) first documented the effect for subsurface water movement of a coarse sand layer underlying a fine soil. If a wetting front reaches the interface the water is held in the pores of the fine soil due to large adhesive and cohesive forces. The pores of the coarser material may not hold water at the tension which exists in the wetting fine material above. The vertical extend of water is limited until the fine material becomes sufficiently saturated and reaches the water entry value of the coarse material. The water entry value is equivalent to the matric potential at which air in the pores is initially displaced by water in a dry porous medium (Wang et al., 2000; Hillel and Baker, 1988). As soon as the fine material gets wet enough, the capillary force will no longer prevent the water from entering the coarse layer (Ross, 1990).

Since it is the mechanism of capillary tension that is responsible for a limitation of vertical seepage, this effect is referred to as the capillary barrier (Stormont and Anderson, 1999; Ross, 1990). Given a horizontal interface, the wetting front will temporarily pause. After reaching the threshold of water entry the water will continue to percolate into the coarse layer spatially concentrated as a finger-shaped flow, due to the higher conductivity that exceed the supply rate from the overlying fine layer (Hillel and Baker, 1988). Within a sloping layered system, the water prevented from entering the coarser material may be suspended above the interface and diverted downslope according to the slope inclination of the interface (Morii et al., 2014; Stormont, 1996; Ross, 1990; Miyazaki, 1988). Kung (1993, 1990) referred to the flow along a capillary barrier as funnel flow.

Transferring these concept to our layered slope material, the interface between the very coarse and highly conductive material of the LB2 and the low conductive and fine material of the LB1 may act as capillary barrier under unsaturated conditions. This is in good agreement with the findings of Heller and Kleber (2016); Hübner et al. (2015); Chifflard et al. (2008); Kleber and Schellenberger (1998), who show the time variable impact of the LB as impeding layer for vertical seepage, which layer also acts as a significant pathway for subsurface stormflow. Due to the multi part structure of the LB at our test plot, this variable impact is limited to the LB2 part of the LB. With low pre–moisture and low amount of precipitation the vertical flow is limited at the interface to the LB2. The water may be impeded to enter the LB2 and is stored within the LB1. As soon as the LB1 gets sufficiently saturated during a rain event, e.g. through high pre–moisture, high precipitation amount or high rain intensity, and the seepage water may not be diverted laterally, the matric potential may reach the water entry value of the LB2. The water may no longer be hold by capillary forces and the capillary barrier becomes ineffective. The water is able to enter the LB2 and due to the hydraulic properties (e.g. high hydraulic conductivity and anisotropy) of the LB2 material it may contribute crucially to the rapid runoff component as subsurface stormflow within the LB2.

Due to the dry initial conditions of the LB1 at the beginning of the first irrigation the interface of the LB2 acts as capillary barrier and the infiltration is restricted to shallow depth. With increasing supply of water the maintaining capillary barrier effect triggers a lateral flow above the sloping interface to the LB2. This is the case when the water of the first irrigation reaches the interface to the LB2. The water is deflected and the flow vector changes from the vertical into the lateral downslope direction. With a short delay of approx. 30 min to the 0.6 m depth, an increase in water content is recorded in 0.85 m depth in

the downslope direction (Tab: 2). The results show significant lateral water movement within the entire LB1, although the LB1 is the layer with the lowest amount of macropores and the lowest hydraulic conductivity.

Under continuous supply of water from the surface the volume of the laterally diverted water increases in the downslope direction. After a certain distance the matric potential of the fine material ~~will become~~ sufficiently less negative and the water starts to percolate into the coarser material (Ross, 1990; Walter et al., 2000). The ERT results show that the plume spreads further into deeper parts in the downslope direction (Fig. 6 - 305 min and Fig. 8), whereas it is limited to shallow parts beneath the irrigation plot (Fig. 8). Despite the limited irrigation area, due to the high irrigation intensity and the lateral water diversion beneath the irrigation plot the volume of water increases downslope. Therefore, the saturation of the LB1 increases in the downslope direction with time. At the time when the matric potential of the LB1 ~~reach~~ the water entry point of the LB2, the capillary barrier effect ~~could not~~ be maintained and the water is able to drain into deeper parts. This is also confirmed by the hydrometric results. After approx. 5h from the beginning of the first irrigation, the matric potential at the depth range of the LM and the LB1 (0.6 and 0.85 m) indicates saturated conditions. Almost simultaneously at 1.2 and 1.5 m depth the first increase in water content is registered (Fig. 4). Through following vertical water supply at 1.2 m depth, saturated conditions are reached 1h30min after the end of the irrigation. In contrast, the supply is not sufficient to achieve saturation at 1.5 m depth. This may be due to a higher hydraulic conductivity at 1.5 m depth than at 1.2 m depth. The water drains faster through the deeper part than it is ~~able to be~~ supplied. This confirms the high hydraulic conductivity, which was estimated in the trench (Tab. 1).

Almost immediately after the end of the first irrigation the matric potential at 0.6 m depth decreases (Tab. 2). Given this short time delay, it has to be hydraulically connected to the irrigation surface indicating steady state conditions. In the other depth ranges it lasts 43 min up to 180 min after the irrigation has been terminated, before the matric potential starts to decrease again. Subsequent water flow still causes changes, suggesting that no steady state conditions ~~were~~ achieved. Between the two irrigations the changes in moisture are diminishing constantly but do not attain the initial conditions of the first irrigation. Field capacity may be assumed at the beginning of the second irrigation because this is referred to be the water content which is held against gravitation two to three days of free drainage after infiltration, typically at a matric potential of -33 hPa (Coleman, 1947; Veihmeyer and Hendrickson, 1931).

The infiltration and the water movement during the second irrigation show very similar processes (Fig. 7). The LH is characterized by preferential flow, whereas the water flow within the LM and the LB1 is approximately uniform. First, vertical infiltration dominates until the water reaches the interface to the LB2 (Fig. 7 - 47 min). The water is deflected, which causes lateral water movement within the LB1 downslope. At about the time of saturation within the LB1, the start of the breakthrough into the LB2 ~~was~~ recorded (Tab. 3). The main difference resides in the flow velocity. Due to the initial conditions near field capacity the water movement is significantly faster than during the first irrigation. After 3h the subsurface down to 1.2 m depth, except for the depth range of the LH, is saturated (Fig. 4). At this point in time the water movement already reached an extent comparable to the final stage of the first irrigation (cf. Fig. 6 - 375 min and Fig. 7 - 187 min). The increased and faster volume of seepage water enables the involved depth ranges to achieve steady state conditions. At 1.5 m distance all depths ≥0.6 m indicate steady state during the second irrigation. They are hydraulically well connected to the irrigation surface. Few minutes after the irrigation has been stopped, the apex of the matric potential curve was recorded at all depths (Tab. 3). Due to the

moister initial conditions, less water is retained and the plume may extend further downslope or into deeper parts. The reaction at the second distance (2.5 m) is limited to the LM and the LB1 (Fig. 5). Within the hydrometric results the reaction at 0.6 m is significantly faster than the at 0.85 m depth (Tab. 3). The ERT results may not confirm this difference in general (Fig. 5). This might be a problem of the punctual characteristic of the hydrometric devices. As shown in the top views (Fig. 6 and Fig. 7) the spread in the downslope direction is conical-shaped, symmetrical to the centre of the irrigation area. The closer the position to the centre, the faster the reaction.

Since the first and second irrigation experiments show comparable results only with differences in time response, some general information about the involved spatial processes and the disparate behaviour of the individual layers may be drawn (Fig. 10).

The high infiltration capacity of the organic layer prevents the occurrence of overland flow but supports the development of organic layer interflow (Fig. 10: OLIF). The infiltration into the LH proceeds fast and is dominated by preferential flow (Fig. 10: PF). Despite the differences in bulk density and pore distribution, there is no evidence of subsurface stormflow at the interface between the LH and the LM. However, a shift in the type of water movement from a dominance of preferential towards a dominance of matric flow takes place at this interface. In the LM and the LB1 the orientation of water movement changes from the vertical to the downslope direction. These two layers are the main region for subsurface stormflow. Within the LM it is mainly caused by changes in hydraulic properties at the interface to the LB1 (Fig. 10: SSF1), whereas the subsurface stormflow of the LB1 is a result of the capillary barrier effect at the interface to the LB2 (Fig. 10: SSF2). The capillary barrier effect prevents water from entering the LB2 in the "capillary diversion" region. Downslope the matric potential within the LB1 becomes sufficiently high due to following water from downslope and from the vertical direction. This enables water to enter the LB2 in the "breakthrough" region and may ease an additional subsurface stormflow within the LB2 (Fig. 10: SSF3).

This concept of water movement derived from the irrigation experiments are subject to restrictions on transferability to the catchment scale. In small headwater catchments the precipitation normally covers the entire catchment. Therefore the infiltration under natural conditions is spatially not as limited as our irrigation area. As a result to the supply from the entire surface, the break-down of a capillary barrier would be more extensive. For a continuous capillary barrier, different flow regimes may occur and alternate along the interface: "capillary diversion", "partial" or "complete breakthrough" and "toe diversion" (Walter et al., 2000; Heilig et al., 2003). The length of the diversion strongly depends on hydraulic conductivity of the fine material, the slope of the interface as well as the infiltration rate (Ross, 1990). For our experiment with this high rain intensity the diversion capacity of the capillary barrier is to be expected to be less effective than under natural conditions with usually lower rain intensity.

Under the assumption that large areas of the catchment are covered by a layered system consisting of a fine-grained layer (FL - such as LB1) overlying a coarse-grained layer (CL - such as LB2), a capillary barrier would significantly influences the response time of the catchment. Amount and intensity of rain, as well as the pre–moisture of the FL are the crucial key features determining the activation of different flow pathways of the subsurface. With low pre–moisture and low amount or intensity of rain a capillary barrier would prevent water from entering the CL and an increased outflow of the catchment would mainly originate from subsurface stormflow within the FL. Due to the low hydraulic conductivity and storage capacity of an

unsaturated FL, this could only cause a slow slightly increased runoff (see Heller and Kleber (2016) pre–moisture controlled type 1 – low pre–moisture). With moderate saturation of the FL or a high amount or intensity of precipitation the capillary barrier would temporarily delay the activation of the CL as flow pathway. This would result in a slowly increasing outflow at an early stage, due to lateral water movement within the organic layer or the FL. With progressing saturation of the FL the capillary barrier might break down and activate the CL as a significant pathway for subsurface stormflow. Subsequently, the rapid water movement within the CL would cause a fast and ~~strong~~ increased runoff (see Heller and Kleber (2016) pre–moisture controlled type 2 - intermediate pre–moisture). On the contrary, with a FL with a high pre–event moisture content a formation of a capillary barrier might be negligible. Seepage water may induce a rapid saturation of the FL and the capillary barrier ~~becomes~~ ineffective. With high pre–moisture an early activation of the CL results in a fast and strong catchment response to precipitation (see Heller and Kleber (2016) pre–moisture controlled type 3 – high pre–moisture). The onset time depends on the intensity of rain. The higher the intensity the faster the response. However, smaller rain events may cause a significant increase in runoff due the faster activation of deeper pathways.

## 5    Conclusions

With a multi-technical approach of using 3D ERT measurements in combination with hydrometric data we were able to identify some principles of water movement in layered slope deposits during two irrigation experiments. Both irrigation experiments show similar results but with differences in time response caused by the higher pre–moisture conditions of the second irrigation.

The highly conductive organic layer prevents overland flow but also supports the occurrence of organic layer interflow. Due to the loose and heterogeneous bedding with a high amount of macro pores, the uppermost layer (LH) is characterized by a high hydraulic conductivity. The infiltration does not proceed ~~uniform~~ but rather as preferential flow. Thus the water percolates rapidly down to the second layer at approx. 0.5m depth. Although this layer exhibits a higher bulk density and a very low hydraulic conductivity, the seepage water is not impeded. There are no evidences for an occurrence of subsurface stormflow at the interface from the LH to the LM. The water may easily enter the LM and spread uniformly down to the LB1. Through the change of sedimentological and hydraulic properties between the LM and the LB1, a proportion of the seepage water is impeded, resulting in the formation of subsurface stormflow above this interface. The remaining water percolates as a uniform wetting front down to the LB2. At approx. 1.1 m depth at the interface to the LB2, the water is prevented from further downward percolation. By the diverging grain size distributions of the sandy LB1 with moderate percentage of gravel and the very coarse LB2 full of large debris, the interface provides a sharp contrast in the functional relationship between saturation and matric potential and, accordingly, hydraulic conductivity. For this reason the interface to the LB2 acts as a capillary barrier under the present unsaturated conditions. The water does not enter the LB2 and, consequently, with increasing supply it becomes deflected in the downslope direction depending on the slope inclination. This causes subsurface stormflow within the LB1. Therefore, the main deep range for subsurface stormflow is limited to the layers with the lowest hydraulic conductivities at 0.5 to 1.1 m. To percolate into the LB2, the matric potential of the overlying finer–pored LB1 has to reach the water entry value of the coarse–pored LB2. Under continuous supply from the surface, the volume of water along the capillary barrier increases

downslope with time. Almost at the time of saturation in the main subsurface stormflow deep range, the first breakthrough is recorded into the LB2. Therefore, the water flow along the capillary barrier may be split into two regions. First the "capillary diversion" beneath the irrigated plot, where no change in depth >1.1 m could be observed. Second, the "breakthrough region" where the capillary barrier could not be maintained and the water is able to drain into deeper parts.

The variable formation and break down of a capillary barrier highlights the alternating impact for subsurface water flow. The activation or prevention of different flow pathways in layered slope deposits, where a fine layer overlies a coarse layer, may be significantly influenced by a capillary barrier. ~~An existing~~ capillary barrier may prevent water from deeper percolation and contributes to the formation of subsurface stormflow above. Whether and to what extend a capillary barrier separates the water flow from the underlying layer depends slope inclination, amount and intensity of rainfall as well as the pre–moisture conditions of the overlying layers. With an active barrier the response time of a catchment is reduced, because the main subsurface runoff is limited to the finer layers with less hydraulic conductivity. With the partial or complete breakdown of the barrier the response time increases rapidly because of the activation of coarser layers with higher hydraulic conductivities.

*Acknowledgements.* We are very grateful to Silvio Gesellmann for grain size analysis. For article processing charges we acknowledge financial support by the German Research Foundation and the Open Access Publication Funds of the TU Dresden.

# References

Alfieri, L., Burek, P., Feyen, L., and Forzieri, G.: Global warming increases the frequency of river floods in Europe, Hydrology and Earth System Sciences, 19, 2247–2260, doi:10.5194/hess-19-2247-2015, 2015.

Ali, G., Tetzlaff, D., McDonnell, J. J., Soulsby, C., Carey, S., Laudon, H., McGuire, K., Buttle, J., Seibert, J., and Shanley, J.: Comparison of threshold hydrologic response across northern catchments, Hydrological Processes, 29, 3575–3591, doi:10.1002/hyp.10527, 2015.

Anderson, M. G. and Burt, T. P., eds.: Process studies in hillslope hydrology, Wiley, Chichester, West Sussex, England; New York, 1990.

Bechtold, M., Vanderborght, J., Weihermueller, L., Herbst, M., Günther, T., Ippisch, O., Kasteel, R., and Vereecken, H.: Upward Transport in a Three-Dimensional Heterogeneous Laboratory Soil under Evaporation Conditions, Vadose Zone Journal, 11, doi:10.2136/vzj2011.0066, 2012.

Beff, L., Günther, T., Vandoorne, B., Couvreur, V. & Javaux, M. (2013): Three-dimensional monitoring of soil water content in a Maize field using Electrical Resistivity Tomography. - Hydrology and Earth System Sciences, 17, 595–609, doi:10.5194/hess-17-595-2013.

Binley, A., Shaw, B., and Henry-Poulter, S.: Flow pathways in porous media: Electrical resistance tomography and dye staining image verification, Measurement Science and Technology, 7, 384–390, doi:10.1088/0957-0233/7/3/020, 1996.

Cassiani, G., Godio, A., Stocco, S., Villa, A., Deiana, R., Frattini, P., and Rossi, M.: Monitoring the hydrologic behaviour of a mountain slope via time-lapse electrical resistivity tomography, Near Surface Geophysics, 7, 475–486, doi:10.3997/1873-0604.2009013, 2009.

Chifflard, P., Didszun, J., and Zepp, H.: Skalenübergreifende Prozess-Studien zur Abflussbildung in Gebieten mit periglazialen Deckschichten (Sauerland, Deutschland), Grundwasser, 13, 27–41, 2008.

Coleman, E. A.: A Laboratory Procedure for Determining the Field Capacity of Soils, Soil Science, 63, 277–284, doi:10.1097/00010694-194704000-00003, 1947.

Descloitres, M., Ribolzi, O., and Le Troquer, Y.: Study of infiltration in a Sahelian gully erosion area using time-lapse resistivity mapping, Catena, 53, 229–253, doi:10.1016/S0341-8162(03)00038-9, 2003.

DIN 18123: Baugrund, Untersuchung von Bodenproben, Bestimmung der Korngrößenverteilung, German Institute for Standardization, Beuth, 1983.

Doetsch, J., Linde, N., Vogt, T., Binley, A., and Green, A. G.: Imaging and quantifying salt-tracer transport in a riparian groundwater system by means of 3D ERT monitoring, Geophysics, 77, B207–B218, doi:10.1190/GEO2012-0046.1, 2012.

French, H. and Binley, A.: Snowmelt infiltration: monitoring temporal and spatial variability using time-lapse electrical resistivity, Journal of Hydrology, 297, 174–186, doi:10.1016/j.jhydrol.2004.04.005, 2004.

Friedel, S.: Resolution, stability and efficiency of resistivity tomography estimated from a generalized inverse approach, Geophys. J. Int., 153, 305–316, doi:10.1046/j.1365-246X.2003.01890.x, 2003.

Ganz, C., Bachmann, J., Noell, U., Duijnisveld, W. H. M., and Lamparter, A.: Hydraulic Modeling and in situ Electrical Resistivity Tomography to Analyze Ponded Infiltration into a Water Repellent Sand, Vadose Zone Journal, 13, doi:10.2136/vzj2013.04.0074, 2014.

Gardner, W. and Hsieh, J.: Water Movement in Soils, [Video], Washington State University, 1959.

Garré, S., Koestel, J., Günther, T., Javaux, M., Vanderborght, J., and Vereecken, H.: Comparison of Heterogeneous Transport Processes Observed with Electrical Resistivity Tomography in Two Soils, Vadose Zone Journal, 9, 336–349, doi:10.2136/vzj2009.0086, 2010.

Günther, T., Rücker, C., and Spitzer, K.: Three-dimensional modelling and inversion of dc resistivity data incorporating topography - II. Inversion, Geophysical Journal International, 166, 506–517, doi:10.1111/j.1365-246X.2006.03011.x, 2006.

Hayashi, M.: Temperature-Electrical Conductivity Relation of Water for Environmental Monitoring and Geophysical Data Inversion, Environmental Monitoring and Assessment, 96, 119–128, doi:10.1023/B:EMAS.0000031719.83065.6, 2004.

Hübner, R., Heller, K., Günther, T., and Kleber, A.: Monitoring hillslope moisture dynamics with surface ERT for enhancing spatial significance of hydrometric point measurements, Hydrology and Earth System Sciences, 19, 225–240, doi:10.5194/hess-19-225-2015, 2015.

5 Heilig, A., Steenhuis, T. S., Walter, M., and Herbert, S. J.: Funneled flow mechanisms in layered soil: field investigations, Journal of Hydrology, 279, 210–223, doi:10.1016/S0022-1694(03)00179-3, 2003.

Heller, K. and Kleber, A.: Hillslope runoff generation influenced by layered subsurface in a headwater catchment in Ore Mountains, Germany, Environ Earth Sci, 75, doi:10.1007/s12665-016-5750-y, 2016.

Hillel, D. and Baker, R. S.: A Descriptive Theory of Fingering During Infiltration Into Layered Soils, Soil Science, 146, 51–56,
10 doi:10.1097/00010694-198807000-00008, 1988.

Keller, G. V. and Frischknecht, F. C.: Electrical methods in geophysical prospecting, Pergamon Press, Oxford, 1966.

Kemna, A., Kulessa, B., and Vereecken, H.: Imaging and characterisation of subsurface solute transport using electrical resistivity tomography (ERT) and equivalent transport models, Journal of Hydrology, 267, 125–146, doi:10.1016/S0022-1694(02)00145-2, 2002.

Kirkby, M. J., ed.: Hillslope hydrology, Wiley, Chichester, 1980.

15 Kleber, A. and Schellenberger, A.: Slope hydrology triggered by cover-beds. With an example from the Frankenwald Mountains, northeastern Bavaria, Zeitschrift fur Geomorphologie, 42, 469–482, 1998.

Kleber, A. and Terhorst, B., eds.: Mid-latitude slope deposits (cover beds), vol. 66 of *Developments in sedimentology*, Elsevier, 1 edn., 2013.

Koestel, J., Kemna, A., Javaux, M., Binley, A., and Vereecken, H.: Quantitative imaging of solute transport in an unsaturated and undisturbed soil monolith with 3-D ERT and TDR, Water Resources Research, 44, W12 411, doi:10.1029/2007WR006755, 2008.

20 Kung, K.-J.: Preferential flow in a sandy vadose zone: 2. Mechanism and implications, Geoderma, 46, 59 – 71, doi:10.1016/0016-7061(90)90007-V, 1990.

Kung, K.-J. S.: Laboratory Observation of Funnel Flow Mechanism and its Influence on Solute Transport, Journal of Environment Quality, 22, 91, doi:10.2134/jeq1993.00472425002200010012x, 1993.

Kuras, O., Pritchard, J. D., Meldrum, P. I., Chambers, J. E., Wilkinson, P. B., Ogilvy, R. D., and Wealthall, G. P.: Monitoring hy-
25 draulic processes with automated time-lapse electrical resistivity tomography (ALERT), Comptes Rendus Geoscience, 341, 868–885, doi:10.1016/j.crte.2009.07.010, 2009.

LaBrecque, D. J. and Yang, X.: Difference Inversion of ERT Data: a Fast Inversion Method for 3-D In Situ Monitoring, Journal of Environmental and Engineering Geophysics, 6, 83–89, doi:10.4133/JEEG6.2.83, 2001.

Lesmes, D. P. and Friedman, S. P.: Relationships between the Electrical and Hydrogeological Properties of Rocks and Soils, in: Hydrogeo-
30 physics, edited by Rubin, Y. and Hubbard, S. S., pp. 87–128, Springer, Dordrecht, 2006.

Ma, R., McBratney, A., Whelan, B., Minasny, B., and Short, M.: Comparing temperature correction models for soil electrical conductivity measurement, Precision Agriculture, 12, 55–66, doi:10.1007/s11119-009-9156-7, 2011.

McDonnell, J. J.: Where does water go when it rains? Moving beyond the variable source area concept of rainfall-runoff response, Hydrological Processes, 17, 1869–1875, doi:10.1002/hyp.5132, 2003.

35 McDonnell, J. J., Tanaka, T., Mitchell, M. J., and Ohte, N.: Hydrology and biogeochemistry of forested catchments, Hydrological Processes, 15, 1673–1674, doi:10.1002/hyp.351, 2001.

McDonnell, J. J., Sivapalan, M., Vaché, K., Dunn, S., Grant, G., Haggerty, R., Hinz, C., Hooper, R., Kirchner, J., Roderick, M. L., Selker, J., and Weiler, M.: Moving beyond heterogeneity and process complexity: A new vision for watershed hydrology, Water Resources Research, 43, W07 301, 2007.

Michot, D., Benderitter, Y., Dorigny, A., Nicoullaud, B., King, D., and Tabbagh, A.: Spatial and temporal monitoring of soil water content with an irrigated corn crop cover using surface electrical resistivity tomography, Water Resources Research, 39, 1138, doi:10.1029/2002WR001581, 2003.

Miyazaki, T.: Water flow in unsaturated soil in layered slopes, Journal of Hydrology, 102, 201–214, doi:10.1016/0022-1694(88)90098-4, 1988.

Moldenhauer, K.-M., Heller, K., Chifflard, P., Hübner, R., and Kleber, A.: Influence of cover beds on slope hydrology, in: Mid-Latitude Slope Deposits (Cover Beds), edited by Kleber, A. and Terhorst, B., vol. 66 of *Mid-latitude slope deposits (cover beds)*, pp. 127–152, Elsevier, Amsterdam etc., 2013.

Morii, T., Kobayashi, K., Matsumoto, K., and Taguchi, K.: Estimation and observation of water diversion in capillary barrier of soil, in: Unsaturated Soils: Research & Applications, pp. 1197–1203, CRC Press, doi:10.1201/b17034-174, 2014.

Petrow, T. and Merz, B.: Trends in flood magnitude, frequency and seasonality in Germany in the period 1951–2002, Journal of Hydrology, 371, 129 – 141, doi:10.1016/j.jhydrol.2009.03.024, 2009.

Philip, J. R.: Hillslope infiltration: Planar slopes, Water Resources Research, 27, 109–117, doi:10.1029/90WR01704, http://dx.doi.org/10.1029/90WR01704, 1991.

Ramirez, A., Daily, W., LaBrecque, D. J., Owen, E., and Chesnut, D.: Monitoring an underground steam injection process using electrical resistance tomography, Water Resources Research, 29, 73–87, doi:10.1029/92WR01608, 1993.

Rücker, C., Günther, T., and Spitzer, K.: Three-dimensional modelling and inversion of dc resistivity data incorporating topography - I. Modelling, Geophysical Journal International, 166, 495–505, doi:10.1111/j.1365-246X.2006.03010., 2006.

Robinson, D. A., Binley, A., Crook, N., Day-Lewis, F. D., Ferré, T. P. A., Grauch, V. J. S., Knight, R., Knoll, M. D., Lakshmi, V., Miller, R., Nyquist, J., Pellerin, L., Singha, K., and Slater, L.: Advancing process-based watershed hydrological research using near-surface geophysics: A vision for, and review of, electrical and magnetic geophysical methods, Hydrological Processes, 22, 3604–3635, doi:10.1002/hyp.6963, 2008a.

Robinson, D. A., Campbell, C. S., Hopmans, J. W., Hornbuckle, B. K., Jones, S. B., Knight, R., Ogden, F., Selker, J., and Wendroth, O.: Soil moisture measurement for ecological and hydrological watershed-scale observatories: A review, Vadose Zone Journal, 7, 358–389, doi:10.2136/vzj2007.0143, 2008b.

Ross, B.: The diversion capacity of capillary barriers, Water Resources Research, 26, 2625–2629, doi:10.1029/WR026i010p02625, 1990.

Sauer, D., Scholten, T., and Felix-Henningsen, P.: Verbreitung und Eigenschaften periglaziärer Lagen im östlichen Westerwald in Abhängigkeit von Gestein, Exposition und Relief, Mitteilungen der Bodenkundlichen Gesellschaft, 96, 551–552, 2001.

Scaini, A., Audebert, M., Hissler, C., Fenicia, F., Gourdol, L., Pfister, L., and Beven, K. J.: Velocity and celerity dynamics at plot scale inferred from artificial tracing experiments and time-lapse ERT, Journal of Hydrology, 546, 28 – 43, doi:10.1016/j.jhydrol.2016.12.035, 2017.

Schmocker-Fackel, P. and Naef, F.: More frequent flooding? Changes in flood frequency in Switzerland since 1850, Journal of Hydrology, 381, 1 – 8, doi:10.1016/j.jhydrol.2009.09.022, 2010.

Seibert, J. and van Meerveld, I.: Hydrological change modeling: Challenges and opportunities, Hydrological Processes, doi:10.1002/hyp.10999, 2016.

Semmel, A. and Terhorst, B.: The concept of the Pleistocene periglacial cover beds in central Europe: A review, Quaternary International, 222, 120 – 128, doi:10.1016/j.quaint.2010.03.010, 2010.

Sinai, G. and Dirksen, C.: Experimental evidence of lateral flow in unsaturated homogeneous isotropic sloping soil due to rainfall, Water Resources Research, 42, W12 402, doi:10.1029/2005WR004617, 2006.

Singha, K. and Gorelick, S. M.: Saline tracer visualized with three-dimensional electrical resistivity tomography: Field-scale spatial moment analysis, Water Resources Research, 41, W05 023, doi:10.1029/2004WR003460, 2005.

Stormont, J. C.: The effectiveness of two capillary barriers on a 10% slope, Geotechnical & Geological Engineering, 14, 243–267, doi:10.1007/BF00421943, 1996.

Stormont, J. C. and Anderson, C. E.: Capillary Barrier Effect from Underlying Coarser Soil Layer, Journal of Geotechnical and Geoenvironmental Engineering, 125, 641–648, doi:10.1061/(ASCE)1090-0241(1999)125:8(641), 1999.

Tetzlaff, D., Birkel, C., Dick, J., Geris, J., and Soulsby, C.: Storage dynamics in hydropedological units control hillslope connectivity, runoff generation, and the evolution of catchment transit time distributions, Water Resources Research, 50, 969–985, doi:10.1002/2013WR014147, 2014.

Travelletti, J., Sailhac, P., Malet, J.-P., Grandjean, G., and Ponton, J.: Hydrological response of weathered clay-shale slopes: water infiltration monitoring with time-lapse electrical resistivity tomography, Hydrological Processes, 26, 2106–2119, doi:10.1002/hyp.7983, 2012.

Uchida, T., McDonnell, J. J., and Asano, Y.: Functional intercomparison of hillslopes and small catchments by examining water source, flowpath and mean residence time, Journal of Hydrology, 327, 627–642, doi:10.1016/j.jhydrol.2006.02.037, 2006.

Uhlemann, S., Thieken, A. H., and Merz, B.: A consistent set of trans-basin floods in Germany between 1952-2002, Hydrology and Earth System Sciences, 14, 1277–1295, doi:10.5194/hess-14-1277-2010, 2010.

Uhlenbrook, S., Didszun, J., and Wenninger, J.: Source areas and mixing of runoff components at the hillslope scale - A multi-technical approach, Hydrological Sciences Journal, 53, 741–753, doi:10.1623/hysj.53.4.741, 2008.

Veihmeyer, F. J. and Hendrickson, A. H.: The moisture equivalent as a measure of the field capacity of soils, Soil Science, 32, 181–194, doi:10.1097/00010694-193109000-00003, 1931.

Völkel, J., Leopold, M., Mahr, A., and Raab, T.: Zur Bedeutung kaltzeitlicher Hangsedimente in zentraleuropäischen Mittelgebirgslandschaften und zu Fragen ihrer Terminologie, Petermanns Geographische Mitteilungen, 146, 50–59, 2002.

Walter, M. T., Kim, J.-S., Steenhuis, T. S., Parlange, J.-Y., Heilig, A., Braddock, R. D., Selker, J. S., and Boll, J.: Funneled flow mechanisms in a sloping layered soil: Laboratory investigation, Water Resources Research, 36, 841–849, doi:10.1029/1999WR900328, 2000.

Wang, Z., Wu, L., and Wu, Q.: Water-entry value as an alternative indicator of soil water-repellency and wettability, Journal of Hydrology, 231–232, 76 – 83, doi:10.1016/S0022-1694(00)00185-2, 2000.

Wenninger, J., Uhlenbrook, S., Tilch, N., and Leibundgut, C.: Experimental Evidence of Fast Groundwater Responses in a Hillslope/Floodplain Area in the Black Forest Mountains, Germany, Hydrological Processes, 18, 3305–3322, doi:10.1002/hyp.5686, 2004.

Zangar, C. N.: Theory and problems of water percolation., no. 8 in Enineering Monographs, Technical Information Office, Denver Ferderal Center, 1953.

Zhang, Q., Gu, X., Singh, V. P., Sun, P., Chen, X., and Kong, D.: Magnitude, frequency and timing of floods in the Tarim River basin, China: Changes, causes and implications, Global and Planetary Change, 139, 44–55, doi:10.1016/j.gloplacha.2015.10.005, 2016.

**List of Figures**

**Figure 1.** Experimental Setup: a) Schematic overview of subsurface layers (LH, LM, LB1, LB2), with measured electrode and tensiometer positions and irrigation area, b) ERT electrodes, colours marking the three measuring grids.
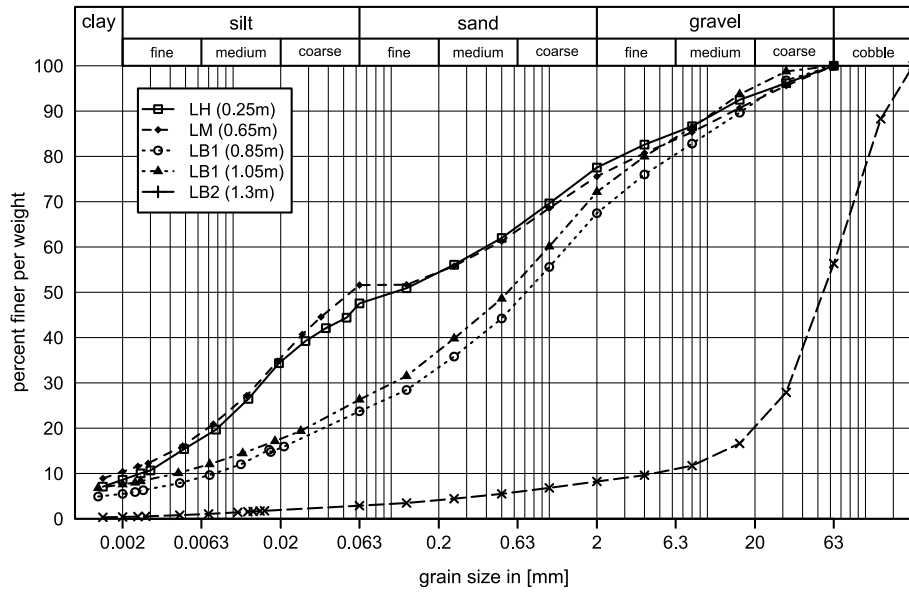
**Figure 2.** Grain size distribution of samples from the trench at different depths.
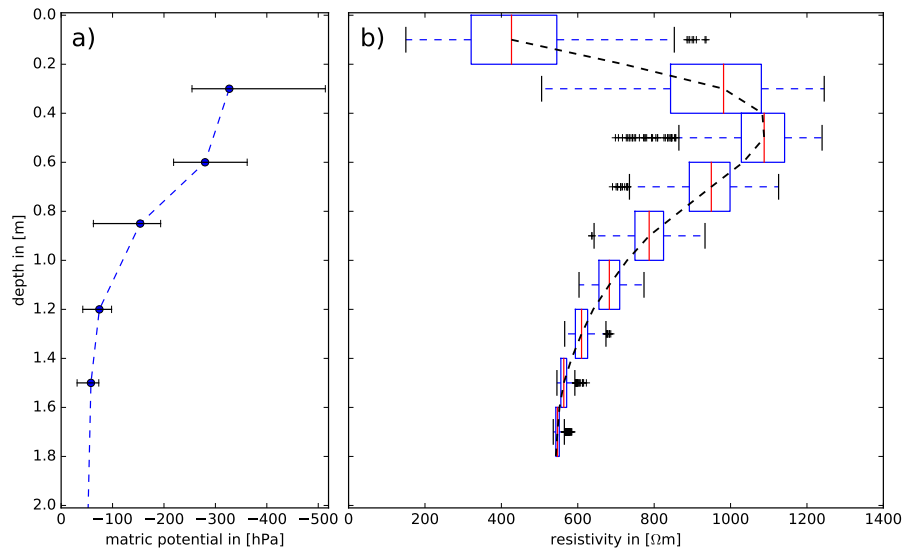
**Figure 3.** Average initial matric potential (a) with range of variation and statistical distribution of resistivity (b) as a function of depth for eight 0.2 m thick depth ranges.
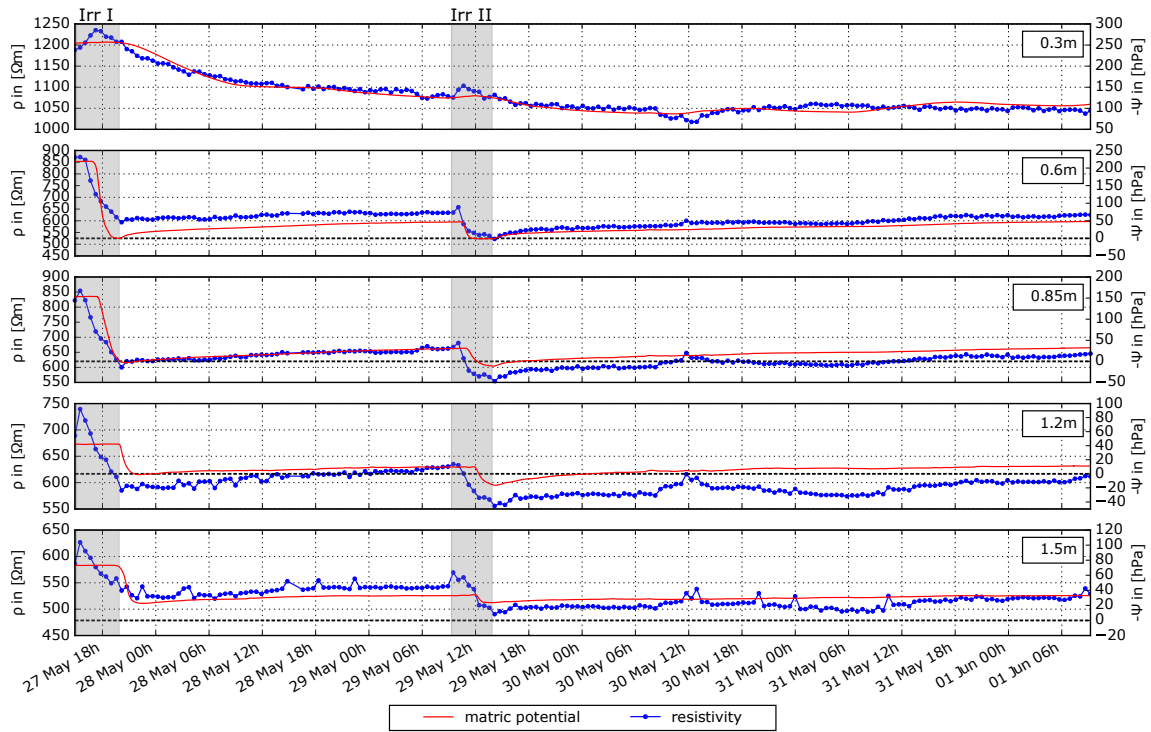
**Figure 4.** Variation of matric potential and co-located resistivity at different depths in 1.5 m distance downslope of the irrigation area (bold dashed lines highlight the 0 hPa level).
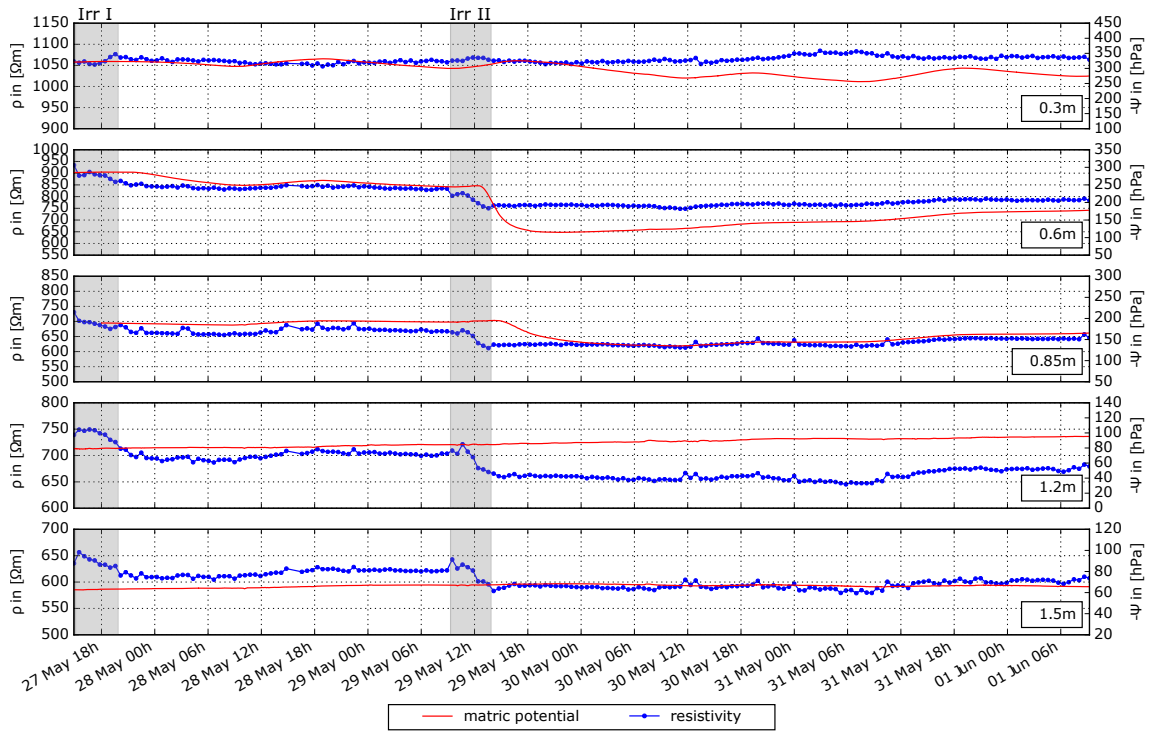
**Figure 5.** Variation of matric potential and co-located resistivity at different depths in 2.5 m distance downslope of the irrigation area.
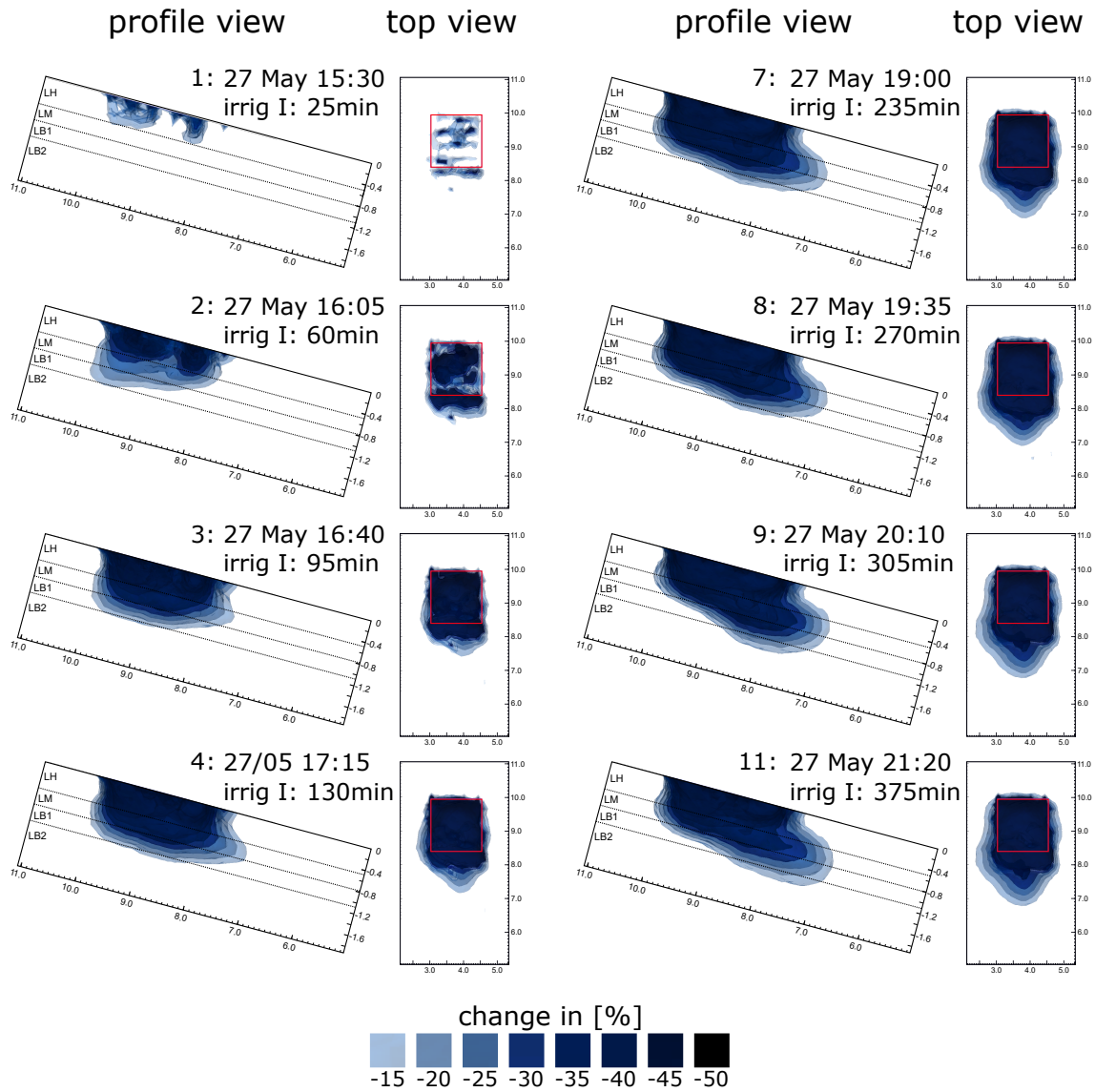
**Figure 6.** Spatial distribution of resistivity change (profile and top view of the 3D model with transparent iso-surfaces and a threshold of 15%) for selected time steps during the first irrigation.
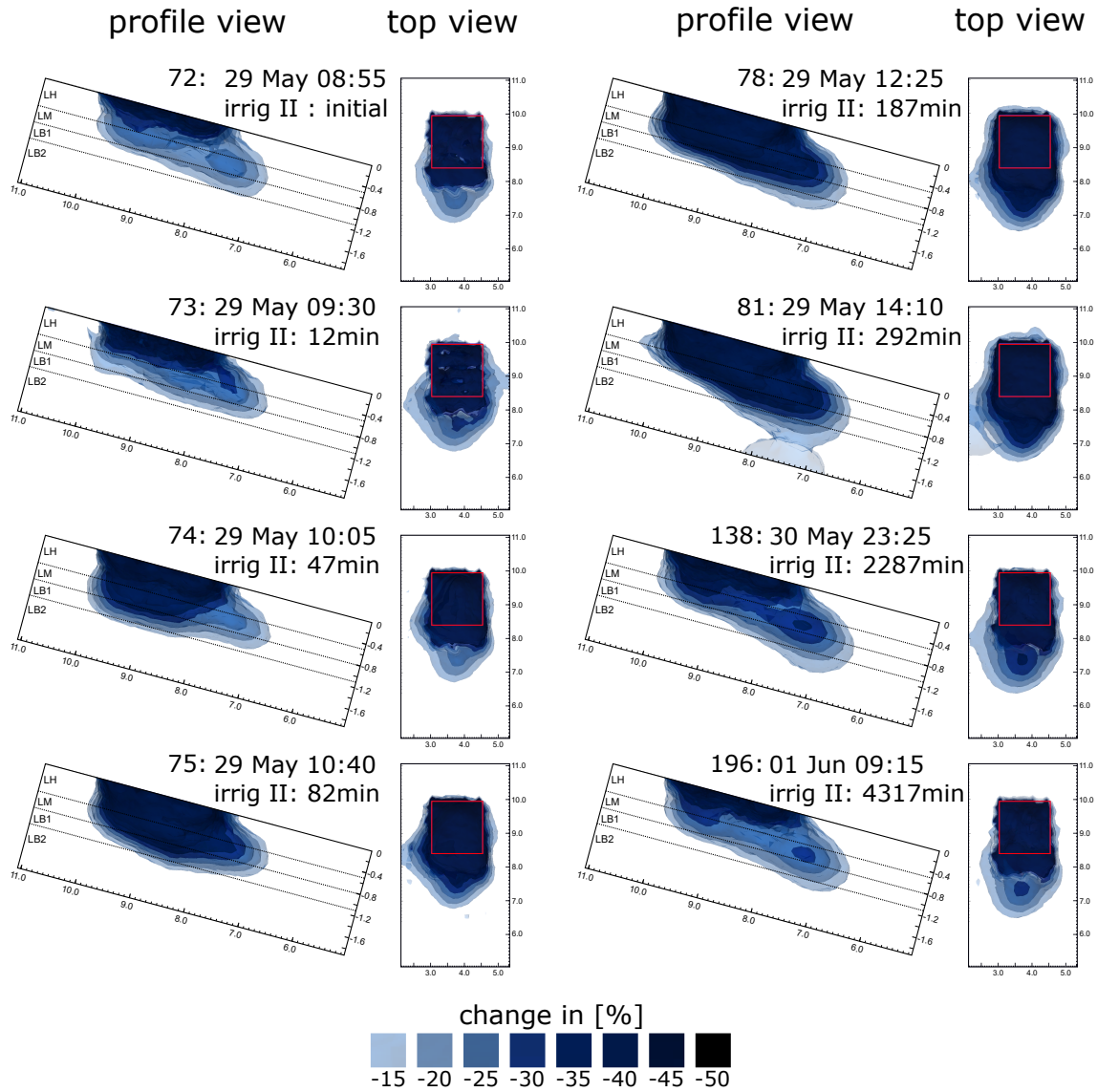
**Figure 7.** Spatial distribution of resistivity change (profile and top view of the 3D model with transparent iso-surfaces and a threshold of 15%) for selected time steps during the second irrigation.
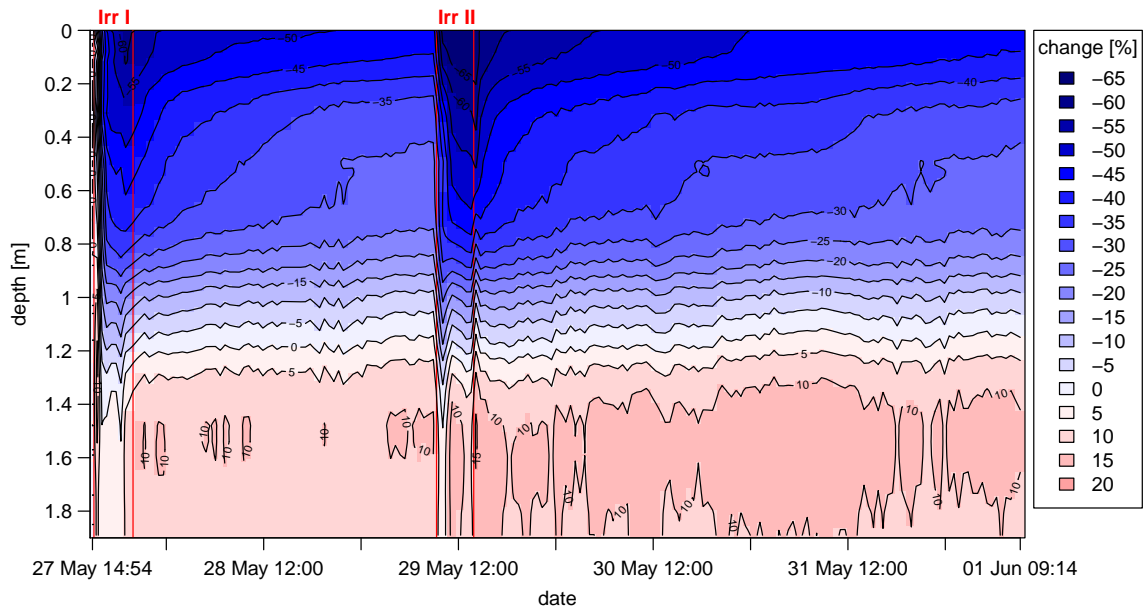
**Figure 8.** Chronological sequence of resistivity change relating to the initial model of a 1D depth profile centrally beneath the irrigation area.
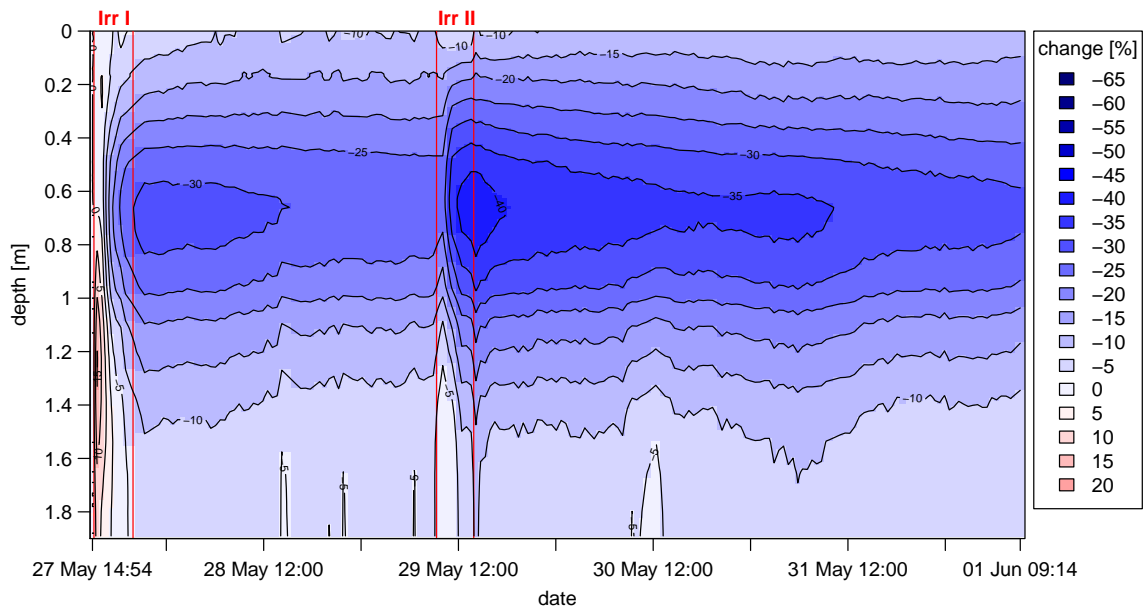
**Figure 9.** Chronological sequence of resistivity change relating to the initial model of a 1D depth profile 1.5 m downslope of the irrigation area.
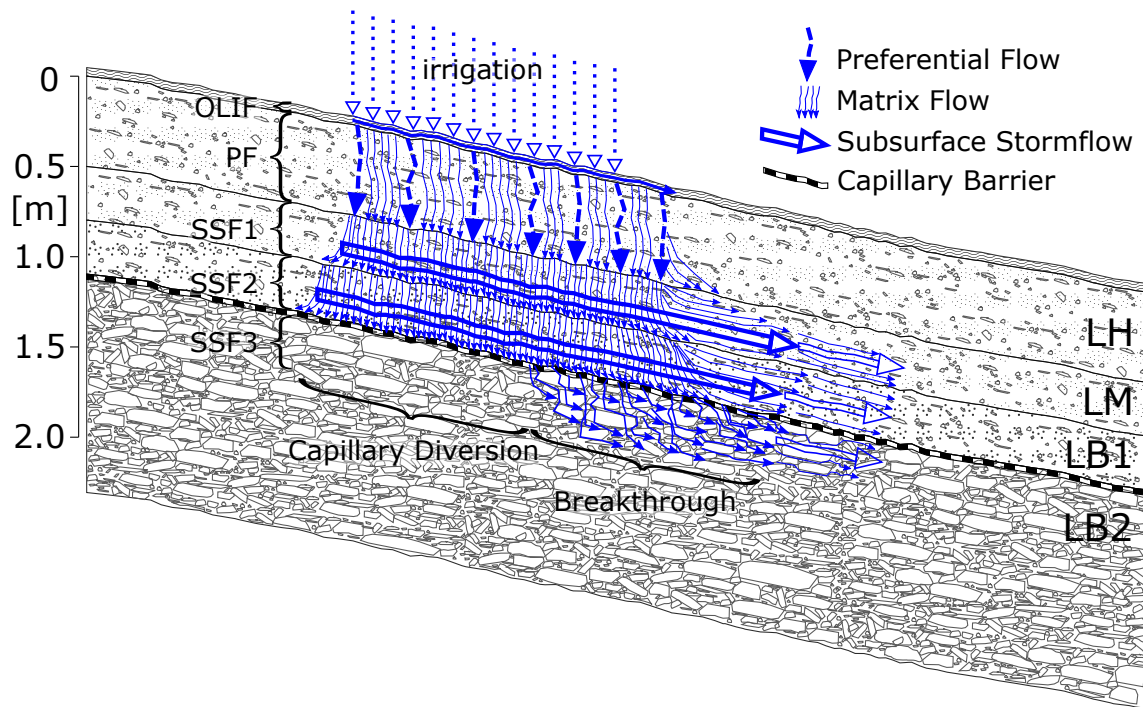
**Figure 10.** Conceptual model of water movement within the individual layers during the irrigation experiments (OLIF - organic layer interflow, PF - preferential flow, SSF - subsurface stormflow)

**List of Tables**

**Table 1.** Sedimentological properties (grain size distribution, bulk density and saturated hydraulic conductivity $K_{sat}$) of the subsurface layers.

| layer | thickness [m] | clay [%] | silt [%] | sand [%] | gravel [%] | cobble [%] | bulk density [g m$^{-3}$] | $K_{sat}$ [cm d$^{-1}$] |
|---|---|---|---|---|---|---|---|---|
| LH | 0.5 | 8.6 | 38.9 | 30.0 | 22.5 | – | 1.14 | 264.55 |
| LM | 0.3 | 10.4 | 41.2 | 24.0 | 24.4 | – | 1.65 | 65.19 |
| LB1 | 0.3 | 6.6 | 18.5 | 44.8 | 30.1 | – | 1.85 | 36.72 |
| LB2 | > 1.4 | 0.4 | 2.5 | 5.3 | 48.1 | 43.7 | – | 2203 |

**Table 2.** Characteristic breakthrough times at different depths for the first irrigation.

Irrigation I May 27. 15:05 pm — 19:54 pm (duration: $4\,\mathrm{h}49\,\mathrm{min} - 670l \approx 61.8\,\mathrm{mm/h}$)

| depth | distance: 1.5 m downslope | | | distance: 2.5 m downslope | | |
|---|---|---|---|---|---|---|
| | start of breakthrough | time to saturation | end of breakthrough | start of breakthrough | time to saturation | end of breakthrough |
| 0.3 | 03 h 33 min | —- | 18 h 55 min | —- | —- | —- |
| 0.6 | 01 h 40 min | 04 h 44 min | 04 h 52 min | 06 h 10 min | —- | 19 h 05 min |
| 0.85 | 02 h 17 min | 04 h 56 min | 05 h 32 min | —- | —- | —- |
| 1.2 | 04 h 54 min | 06 h 31 min | 07 h 27 min | —- | —- | —- |
| 1.5 | 04 h 55 min | —- | 07 h 49 min | —- | —- | —- |

**Table 3.** Characteristic breakthrough times at different depths for the second irrigation.

Irrigation II May 29. 09:18 am — 01:53 pm (duration: $4\,\mathrm{h}35\,\mathrm{min} - 700l \approx 67.9\,\mathrm{mm/h}$)

| depth | distance: 1.5 m downslope | | | distance: 2.5 m downslope | | |
| | start of breakthrough | time to saturation | end of breakthrough | start of breakthrough | time to saturation | end of breakthrough |
|---|---|---|---|---|---|---|
| 0.3 | 02 h40 min | —- | 21 h57 min | —- | —- | —- |
| 0.6 | 01 h15 min | 02 h21 min | 04 h47 min | 03 h16 min | —- | 13 h00 min |
| 0.85 | 01 h38 min | 02 h52 min | 04 h49 min | 05 h20 min | —- | 25 h52 min |
| 1.2 | 02 h37 min | 03 h05 min | 05 h05 min | —- | —- | —- |
| 1.5 | 02 h42 min | —- | 04 h52 min | —- | —- | —- |